

TIPS: Text-Induced Pose Synthesis

Prasun Roy¹, Subhankar Ghosh¹, Saumik Bhattacharya²,
Umapada Pal³, and Michael Blumenstein¹

¹ University of Technology Sydney, Australia

prasun.roy@student.uts.edu.au, subhankar.ghosh@student.uts.edu.au,
michael.blumenstein@uts.edu.au

² Indian Institute of Technology Kharagpur, India

saumik@ece.iitkgp.ac.in

³ Indian Statistical Institute Kolkata, India

umapada@isical.ac.in

<https://prasunroy.github.io/tips>

Abstract. In computer vision, human pose synthesis and transfer deal with probabilistic image generation of a person in a previously unseen pose from an already available observation of that person. Though researchers have recently proposed several methods to achieve this task, most of these techniques derive the target pose directly from the desired target image on a specific dataset, making the underlying process challenging to apply in real-world scenarios as the generation of the target image is the actual aim. In this paper, we first present the shortcomings of current pose transfer algorithms and then propose a novel text-based pose transfer technique to address those issues. We divide the problem into three independent stages: (a) text to pose representation, (b) pose refinement, and (c) pose rendering. To the best of our knowledge, this is one of the first attempts to develop a text-based pose transfer framework where we also introduce a new dataset DF-PASS, by adding descriptive pose annotations for the images of the DeepFashion dataset. The proposed method generates promising results with significant qualitative and quantitative scores in our experiments.

Keywords: Text-guided generation, Pose transfer, GAN, DeepFashion

1 Introduction

Generating novel views of a given object is a challenging yet necessary task for many computer vision applications. Pose transfer is a subclass of the view synthesis problem where the goal is to estimate an unseen view (*target* image) of a person with a particular pose from a given observation (*source* image) of that person. As there can be significant differences between the source and target images, the pose transfer pipeline requires a very accurate generative algorithm to infer both the visible and occluded body parts in the target image. The method also needs to preserve the person’s general appearance, including facial expression, skin color, attire, and background. In particular, the goal is

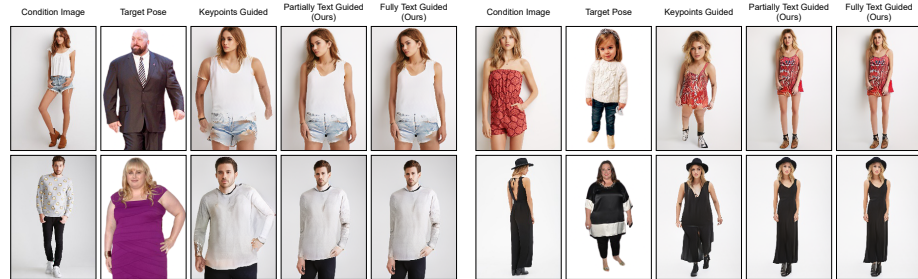


Fig. 1. Overview of the proposed approach. Keypoint-guided methods tend to produce structurally inconsistent images when the physical appearance of the target pose reference significantly differs from the condition image. The proposed text-guided technique successfully addresses this issue while retaining the ability to generate visually decent results close to the keypoint-guided baseline.

to generate a target person image I_B for a specific pose P_B from an input source image I_A of that person having an observed pose P_A . A human pose P is usually expressed by a set of body-joint locations (*keypoints*), denoted as K . As the location of the keypoints can vary significantly from person to person, two different sets of keypoints K and K' may represent the same pose P .

As initial solutions, researchers have introduced coarse to fine generation schemes [28,29] by splitting the problem into separate sub-tasks for handling background, foreground, and pose separately. The architectural complexity of such an approach is later streamlined with a unified pipeline by utilizing deformable GANs [42], variational U-Net [9], and progressive attention transfer [55]. Although the state-of-the-art (SOTA) algorithms have produced visually compelling results, a common yet noticeable flaw is present in these techniques. For training and evaluation of the models, SOTA algorithms extract keypoints K_B directly from I_B to represent P_B and use it as one of the inputs. However, I_B should not be ideally known to users, and such an over-simplified training process creates a dilemma. One way to circumvent the problem is training the model to adapt to a target pose P_B , represented by keypoints K'_B , which is extracted from the image I'_B of some other person. However, as the models are trained using K_B directly, they adapt poorly to any other set of keypoints $K'_B \neq K_B$ representing the same pose P_B . In Fig. 1, we have shown the limitation of the existing keypoint-based models. We use the existing keypoint-guided pose transfer algorithm PATN [55] as a baseline in our experiments. The keypoint-based models try to follow the body structure of the target reference rather than the general pose. Thus, they fail occasionally in the absence of the target image I_B to provide the keypoints. On the other hand, the proposed algorithm is not biased toward the target image as it exclusively works on the textual description of the target pose.

In this paper, we propose a novel pose-transfer pipeline guided by the textual description of the pose. Initially, we estimate the target keypoint set K_B from

the textual description T_B of the target pose P_B . The estimated keypoint set K_B is then used to generate the pose-transferred image \tilde{I}_B . As the estimation of K_B is directly conditioned on T_B , we do not need the target image I_B for estimating the target pose P_B , and the training is free from any bias. The main contributions of our work are as follows.

- We propose a pose transfer pipeline that takes the source image and a textual description of the target pose to generate the target image. To the best of our knowledge, this is one of the first attempts to design a pose transfer algorithm based on textual descriptions of the pose.
- We introduce a new dataset DF-PASS derived from the DeepFashion dataset. The proposed dataset contains a human-annotated text description of the pose for 40488 images of the DeepFashion dataset.
- We extensively explore different perceptual metrics to analyze the performance of the proposed technique and introduce a new metric (GCR) for evaluating the gender consistency in the generated images.
- Most importantly, the algorithm is designed not to require the target image at the time of inference, making it more suitable for real-world applications than the existing pose transfer algorithms.

2 Related Work

Novel view synthesis is an intriguing problem in computer vision. Recently, Generative Adversarial Networks (GANs) [10] have been explored extensively for perceptually realistic image generation [10,17,20,21,31,36]. Conditional generative models [16,31,41,54] have become popular in different fields of computer vision, such as inpainting [46], super-resolution [8,18] etc. Pose transfer can be viewed as a sub-category of the conditional generation task where a target image is generated from a source image by conditioning on the target pose. Thus, with the progress of conditional generative models, pose transfer algorithms have significantly enhanced performance in the last decade. Initial multi-stage approaches divide the complex task into relatively simpler sub-problems. In [50], Zhao *et al.* adopt a coarse to fine approach to generate multi-view images of a person from a single observation. Ma *et al.* [28,29] introduce a multi-stage framework to generate the final pose-transferred image from a single source image. Balakrishnan *et al.* [3] propose a method of pose transfer by segmenting and generating the foreground and background individually. Wang *et al.* [44] introduce a characteristic preserving generative network with a geometric matching module. The coarse to fine generation technique is further improved by incorporating the idea of disentanglement [29] where the generative model is designed as a multi-branch network to handle foreground, background, and pose separately. In [34], the authors propose a pose conditioned bidirectional generator in an unsupervised multi-level generation strategy. In [55], the authors introduce a progressive attention transfer technique to transfer the pose gradually. Li *et al.* [22] propose a method to progressively select important regions of an image using pose-guided

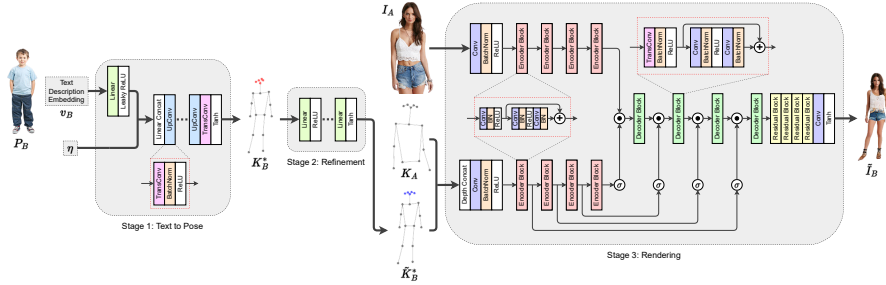


Fig. 2. Architecture of the proposed pipeline. The workflow is divided into three stages. In stage 1, we estimate a spatial representation K_B^* for the target pose P_B from the corresponding text description embedding v_B . In stage 2, we regressively refine the initial estimation of the facial keypoints to obtain the refined target keypoints \tilde{K}_B^* . Finally, in stage 3, we render the target image \tilde{I}_B by conditioning the pose transfer on the source image I_A having the keypoints K_A corresponding to the source pose P_A .

non-local attention with a long-range dependency. Researchers have also investigated 3D appearance flow [23], pose flow [51], and surface-based modeling [11,33] for pose transfer. In [47], the authors first approximate a 3D mesh from a single image, and then the 3D mesh is used to transfer the pose. Siarohin *et al.* [42] propose a nearest neighbour loss for pose transfer using deformable GANs. In [6,53], the authors generate talking-face dynamics from a single face image and a target audio signal.

Text-based image generations are also an intriguing topic in computer vision. In [37], the authors propose a GAN-based architecture for synthesizing the images. Qiao *et al.* [35] have incorporated redescription of textual descriptions for image synthesis. Recently, text-based approaches are also explored for generating human pose [4] and appearance [49]. In [24], the authors use a Variational Autoencoder (VAE) to generate human actions from text descriptions. In [4], the authors generate 3D human meshes from text using a recurrent GAN and SMPL [27] model. In [52], the authors propose a text-guided method for generating human images by selecting a pose from a set of eight basic poses, followed by controlling the appearance attributes of the selected basic pose. However, text-based visual generation techniques are limited in the literature, and text-guided pose transfer is not well-explored previously to the best of our knowledge.

3 Methodology

The proposed technique is divided into three independent sequential stages, each specific to a particular task. In the first stage, we derive an initial estimation of the target pose from the corresponding text description embedding. This coarse pose is then refined through regression at the next step. Finally, pose transfer is performed by conditioning the transformation on the appearance of the source image. We show our integrated generation pipeline in Fig. 2.

3.1 Text to Keypoints Generation

For a given source image I_A , our algorithm aims to generate the pose-transferred image I_B where the target pose P_B is described by textual description T_B . At first, we encode T_B into an embedded vector v_B either by many-hot encoding or using a pre-trained NLP model such as BERT [7], FastText [2], or Word2Vec [30]. We first aim to estimate the keypoint set K_B from v_B using a generative model to guide the pose transfer process in a later stage. To train such a generative model, we represent the keypoints $k_j \in \mathbb{R}^{m \times n}$ where $k_j \in K; \forall j$ and the domain of both I_A and I_B is $\mathbb{R}^{m \times n}$. As a slight spatial variation of k_j does not change the pose P_B , it is better to represent it with a Gaussian distribution $\mathcal{N}(k_j, \sigma_j)$; $\forall j$ for mitigating the high sparsity in the data. Although for different k_j , the invariance of the pose is valid for different amounts of spatial perturbations, we can assume $\sigma_j = \sigma$, a constant, $\forall j$, if σ_j is small. Such representation of keypoints is often referred to as heatmaps.

Taking motivation from [49], we design a generative adversarial network to estimate the target keypoint set K_B from the text embedding v_B . In our generator G_T , we first project v_B into a 128-dimensional latent space ϕ_B using a linear layer with leaky ReLU activation. To allow some structural variations in the generated poses, we sample a 128-dimensional noise vector $\eta \sim N(\mathbf{0}, I)$, where I is a 128×128 identity matrix. Both ϕ_B and η are linearly concatenated and passed through 4 up-convolution blocks. At each block, we perform a transposed convolution followed by batch normalization [15] and ReLU activation [32]. The four transposed convolutions use 256, 128, 64, and 32 filters, respectively. We produce the final output from G_T by passing the output of the last up-convolution block through another transposed convolution layer with 18 filters and \tanh activation. The final generator output $G_T(v_B, \eta)$ has a spatial dimension of $64 \times 64 \times 18$, where each channel represents one of the 18 keypoints k_j , $j \in \{1, 2, \dots, 18\}$. In our discriminator (*critic*) D_T , we first perform 4 successive convolutions, each followed by leaky ReLU activation, on the 18-channel heatmap. The four convolutions use 32, 64, 128, and 256 filters, respectively. The output of the last convolution layer is concatenated with 16 copies of ϕ_B arranged in a 4×4 tile. The concatenated feature map is then passed through a point convolution layer with 256 filters and leaky ReLU activation. We estimate the final scalar output from D_T by passing the feature map through another convolution layer with a single filter. We mathematically define the objective function for D_T as

$$L_D = -\mathbb{E}_{(x, v_B) \sim p_t, \eta \sim p_\eta} [D_T(x, v_B) - D_T(G_T(\eta, v_B), v_B)] \quad (1)$$

where $(x, v_B) \sim p_t$ is the heatmap and text embedding pair sampled from the training set, $\eta \sim p_\eta$ is the noise vector sampled from a Gaussian distribution, and $G_T(\eta, v_B)$ is the generated heatmap for the given text embedding v_B . Researchers [12] have shown that the WGAN training is more stable if D_T is Lipschitz continuous, which mitigates the undesired behavior due to gradient clipping. To enforce the Lipschitz constraint, we compute gradient penalty as

$$\mathcal{C}_T = \mathbb{E}_{(\tilde{x}, v_B) \sim p_{\tilde{x}, v_B}} [(\|\nabla_{\tilde{x}, v_B} D_T(\tilde{x}, v_B)\|_2 - 1)^2] \quad (2)$$

where $\|\cdot\|_2$ indicates the l_2 norm and \tilde{x} is an interpolated sample between a real sample x and a generated sample $G_T(\eta, v_B)$, i.e., $\tilde{x} = \alpha x + (1 - \alpha)G_T(\eta, v_B)$, where α is a random number, selected from a uniform distribution between 0 and 1. Eq. 2 enforces the Lipschitz constraint by restricting the gradient magnitude to 1. We define the overall objective of D_T by combining equations 1 and 2 as

$$L_{D_T} = L_D + \lambda \mathcal{C}_T \quad (3)$$

where λ is a regularization constant. We keep $\lambda = 10$ in all of our experiments. We mathematically define the objective function for G_T as

$$\begin{aligned} L_{G_T} = & -\mathbb{E}_{\eta \sim p_\eta, v_B \sim p_{v_B}} [D_T(G_T(\eta, v_B), v_B)] \\ & - \mathbb{E}_{\eta \sim p_\eta, v_B^1, v_B^2 \sim p_{v_B}} \left[D_T(G_T(\eta, \frac{v_B^1 + v_B^2}{2}), \frac{v_B^1 + v_B^2}{2}) \right] \end{aligned} \quad (4)$$

where $v_B^1, v_B^2 \sim p_{v_B}$ are text encodings sampled from the training set. The second term in Eq. 4 helps the generator learn from the interpolated text encodings, which are not originally present in the training set.

We estimate the target keypoint set K_B^* from the 18-channel heatmap generated from G_T by computing the maximum activation $\psi_j^{max}, j \in \{1, 2, \dots, 18\}$ for every channel. The spatial location of the maximum activation for the j -th channel determines the coordinates of the j -th keypoint if $\psi_j^{max} \geq 0.2$. Otherwise, the j -th keypoint is considered occluded if $\psi_j^{max} < 0.2$.

3.2 Facial Keypoints Refinement

While G_T produces a reasonable estimate of the target keypoints from the corresponding textual description, the estimation K_B^* is often noisy. The spatial perturbation is most prominent for the facial keypoints (nose, two eyes, and two ears) due to their proximity. Slight positional variations for other keypoints generally do not drastically affect the pose representation. Therefore, we refine the initial estimate of the facial keypoints by regression using a linear fully-connected network N_R (RefineNet). At first, the five facial keypoints $k_i^f, i \in \{1, 2, \dots, 5\}$ are translated by $(k_i^f - k_n)$ where k_n is the spatial location of the nose. In this way, we align the nose with the origin of the coordinate system. Then, we normalize the translated facial keypoints such that the scaled keypoints k_i^s are within a square of span ± 1 and the scaled nose is at the origin $(0, 0)$. Next, we flatten the coordinates of the five normalized keypoints to a 10-dimensional vector v_f and pass it through three linear fully-connected layers, where each layer has 128 nodes and ReLU activation. The final output layer of the network consists of 10 nodes and $tanh$ activation. While training, we augment k_i^s with small amounts of random 2D spatial perturbations and try to predict the original values of k_i^s . We optimize the parameters of N_R by minimizing the mean squared error (MSE) between the actual and the predicted coordinates. Finally, we denormalize and retranslate the predicted facial keypoints. The refined set of keypoints \tilde{K}_B^* is obtained by updating the coordinates of the facial keypoints of K_B^* with the predictions from RefineNet.

3.3 Pose Rendering

To render the final pose-transferred image \tilde{I}_B , we first extract the keypoints K_A from the source image I_A using a pre-trained Human Pose Estimator (HPE) [5]. However, we may also estimate the keypoints K_A^* from the embedding vector v_A for the text description T_A of the source pose P_A . If we compute the keypoints K_A^* from T_A , then the refinement is also applied on K_A^* to obtain the refined source keypoints \tilde{K}_A^* . Thus, depending on the source keypoints selection, we propose two slightly different variants of the method – (a) partially text-guided, where we use HPE to extract K_A and (b) fully text-guided, where we estimate \tilde{K}_A^* using G_T followed by N_R . However, in both cases, the pose rendering step works similarly. For simplicity, we discuss the rendering network using K_A as the notation for the source keypoints. We represent the keypoints K_A and \tilde{K}_B^* as multi-channel heatmaps H_A and \tilde{H}_B , respectively, where each channel of a heatmap corresponds to one particular keypoint.

We adopt an attention-guided conditional GAN architecture [38,39] for the target pose rendering. We take I_A , H_A , and \tilde{H}_B as inputs for our generator network G_S , which produces the final rendered image output \tilde{I}_B as an estimate for the target image I_B . The discriminator network D_S utilizes a PatchGAN [16] to evaluate the quality of the generated image by taking a channel-wise concatenation between I_A and either I_B or \tilde{I}_B . In G_S , we have two downstream branches for separately encoding the condition image I_A and the channel-wise concatenated heatmaps (H_A, \tilde{H}_B). After mapping both inputs to a 256×256 feature space by convolution (kernel size = 3×3 , stride = 1, padding = 1, bias = 0), batch normalization, and ReLU activation, we pass the feature maps through four consecutive encoder blocks. Each block encodes the input feature space by reducing the dimension to half but doubling the number of filters. Each encoder block features a sequence of convolution (kernel size = 4×4 , stride = 2, padding = 1, bias = 0), batch normalization, ReLU activation, and a basic residual block [13]. We combine the encoded feature maps and pass the merged feature space through an upstream branch with four consecutive decoder blocks. Each block decodes the feature space by doubling the dimension but reducing the number of filters by half. Each decoder block features a sequence of transposed convolution (kernel size = 4×4 , stride = 2, padding = 1, bias = 0), batch normalization, ReLU activation, and a basic residual block. We use attention links between encoding and decoding paths at every resolution level to retain coarse and fine attributes in the generated image. Mathematically, for the lowest resolution level, $L = 4$,

$$I_3^\delta = \delta_4(I_4^{\pi^i} \odot \sigma(H_4^{\pi^h}))$$

and for the higher resolution levels, $L = \{1, 2, 3\}$,

$$I_{L-1}^\delta = \delta_L(I_L^{\pi^i} \odot \sigma(H_L^{\pi^h}))$$

where, at the resolution level L , I_L^δ denotes the output of the decoding block δ_L , $I_L^{\pi^i}$ denotes the output of the image encoding block π_L^i , $H_L^{\pi^h}$ denotes the output of the pose encoding block π_L^h , σ is an element-wise *sigmoid* activation

function, and \odot is an element-wise product. Finally, we pass the resulting feature maps through four consecutive basic residual blocks followed by a point-wise convolution (kernel size = 1×1 , stride = 1, padding = 0, bias = 0) with \tanh activation to map the feature space into a $256 \times 256 \times 3$ normalized image \tilde{I}_B .

The optimization objective of G_S consists of three loss components – a pixel-wise l_1 loss $\mathcal{L}_{l_1}^{G_S}$, a discrimination loss $\mathcal{L}_{GAN}^{G_S}$ by D_S , and a perceptual loss $\mathcal{L}_{P_\rho}^{G_S}$ computed using a pre-trained VGG-19 network [43]. We measure the pixel-wise l_1 loss as $\mathcal{L}_{l_1}^{G_S} = \|\tilde{I}_B - I_B\|_1$, where $\|\cdot\|_1$ denotes the l_1 norm or the mean absolute error. We compute the discrimination loss as

$$\mathcal{L}_{GAN}^{G_S} = \mathcal{L}_{BCE}(D_S(I_A, \tilde{I}_B), 1) \quad (5)$$

where \mathcal{L}_{BCE} denotes the binary cross-entropy loss. Finally, we estimate the perceptual loss as

$$\mathcal{L}_{P_\rho}^{G_S} = \frac{1}{h_\rho w_\rho c_\rho} \sum_{x=1}^{h_\rho} \sum_{y=1}^{w_\rho} \sum_{z=1}^{c_\rho} \|q_\rho(\tilde{I}_B) - q_\rho(I_B)\|_1 \quad (6)$$

where q_ρ is the output of dimension $(h_\rho \times w_\rho \times c_\rho)$ from the ρ -th layer of a pre-trained VGG-19 network. We add two perceptual loss terms for $\rho = 4$ and $\rho = 9$ to the objective function. So, in our method, the overall optimization objective for G_S is given by

$$\mathcal{L}_{G_S} = \lambda_1 \mathcal{L}_{l_1}^{G_S} + \lambda_2 \mathcal{L}_{GAN}^{G_S} + \lambda_3 (\mathcal{L}_{P_4}^{G_S} + \mathcal{L}_{P_9}^{G_S}) \quad (7)$$

where λ_1 , λ_2 , and λ_3 denote the weighing parameters for respective loss terms. We keep $\lambda_1 = 5$, $\lambda_2 = 1$, and $\lambda_3 = 5$ in our experiments. Lastly, we define the optimization objective for D_S as

$$\mathcal{L}_{D_S} = \frac{1}{2} \left[\mathcal{L}_{BCE}(D_S(I_A, I_B), 1) + \mathcal{L}_{BCE}(D_S(I_A, \tilde{I}_B), 0) \right] \quad (8)$$

4 Dataset and Training

As this is one of the earliest attempts to perform a text-guided pose transfer, we introduce a new dataset called *DeepFashion Pose Annotations and Semantics* (DF-PASS) to compensate for the lack of similar public datasets. DF-PASS contains a human-annotated textual description of the pose for 40488 images of the DeepFashion dataset [26]. Each text annotation contains (1) the person’s gender (e.g. ‘man’, ‘woman’ etc.); (2) visibility flags of the body keypoints (e.g. ‘his left eye is visible’, ‘her right ear is occluded’ etc.); (3) head and face orientations (e.g. ‘her head is facing partially left’, ‘he is keeping his face straight’ etc.); (4) body orientation (e.g. ‘facing towards front’, ‘facing towards right’ etc.); (5) hand and wrist positioning (e.g. ‘his right hand is folded’, ‘she is keeping her left wrist near left hip’ etc.); (6) leg positioning (e.g. ‘both of his legs are straight’, ‘her right leg is folded’ etc.). We recruit five in-house annotators to acquire the

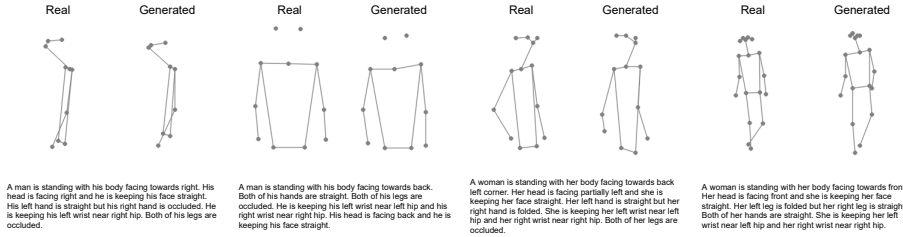


Fig. 3. Qualitative results of text to pose generation using G_T .

text descriptions, which two independent verifiers have validated. Each annotator describes a pose during data acquisition by selecting options from a set of possible attribute states. In this way, we have collected many-hot embedding vectors alongside the text descriptions. We use 37344 samples for training and 3144 samples for testing out of 40488 annotated samples following the same data split provided by [55].

In stage 1, the text to pose conversion network uses the stochastic Adam optimizer [19] to train both G_T and D_T . We keep learning rate $\eta_1 = 1e^{-4}$, $\beta_1 = 0$, $\beta_2 = 0.9$, $\epsilon = 1e^{-8}$, and weight decay = 0 for the optimizer. While training, we update G_T once after every five updates of D_T . In stage 2, we train the facial keypoints refinement network N_R using stochastic gradient descent keeping learning rate $\eta_2 = 1e^{-2}$. In stage 3, the pose rendering network also uses the Adam optimizer to train both G_S and D_S . In this case, we keep learning rate $\eta_3 = 1e^{-3}$, $\beta_1 = 0.5$, $\beta_2 = 0.999$, $\epsilon = 1e^{-8}$, and weight decay = 0. Before training, the parameters of G_T , D_T , G_S , and D_S are initialized by sampling from a normal distribution of 0 mean and 0.02 standard deviation. The code is available at <https://github.com/prasunroy/tips>.

5 Results

In Fig. 3, we demonstrate the output K_B^* of the text to keypoints generator G_T . The textual descriptions used for estimating the respective K_B^* are also shown in the figure. It can be observed that the estimated keypoints K_B^* capture the pose P_B and closely resembles K_B . However, a precise observation may reveal that the facial keypoints of K_B^* significantly differ from K_B . In Fig. 4, the advantage of regressive refinement of keypoints K_B^* is shown. As depicted in the figure, the refinement network aims to rectify only the facial keypoints. In Fig. 5, we demonstrate that when K_B is selected from the DeepFashion dataset, the existing PATN algorithm performs satisfactorily. However, when K_B comes from real-world samples (out of the DeepFashion dataset), PATN fails to generate the pose-transferred images while maintaining structural consistency. In the case of the proposed algorithm, as the pose description does not require structural information of the target image, the generated pose-transferred images are

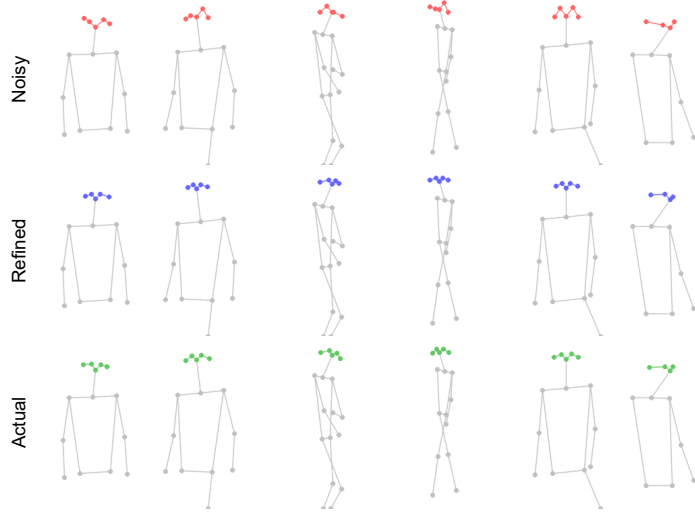


Fig. 4. Qualitative results of regressive refinement using N_R .

consistent with the respective source images. Our proposed algorithm performs well irrespective of the representation of the source pose, i.e., for the partially text-guided approach, where the source pose is represented using keypoints, and for the fully text-guided approach, where the source pose is described using text.

5.1 Evaluation

As the proposed method has three major steps – text to keypoint generation, refinement of the generated keypoints, and generation of the pose-transferred image, it is important to analyze each step qualitatively and quantitatively.

Metrics: Quantifying the generated image quality is a challenging problem. However, researchers [9,28,42,55] have used a few well-known quantitative metrics to judge the quality of the synthesis. This includes a Structural Similarity Index (SSIM) [45], Inception Score (IS) [40], Detection Score (DS) [25], and PCKh [1]. We also evaluate the Learned Perceptual Image Patch Similarity (LPIPS) [48] metric as a more modern replacement of the SSIM for perceptual image quality assessment. In our evaluation, we calculate LPIPS using both VGG19 [43] and SqueezeNet [14] backbones. As we are dealing with human poses and evaluating the generation quality, we propose a novel metric, named Gender Consistency Rate (GCR), that evaluates whether the generated image \tilde{I}_B can be identified to be of the same gender as the source image I_A by a pre-trained classifier. GCR serves two purposes: first, it ensures that the gender-specific features are present in the generated image, and second, it ensures that the generated target image is consistent with the source image. To calculate GCR, we remove the last layer of the VGG19 network and add a single neuron with sigmoid activation to design a binary classifier and train it with the image samples from the DeepFashion



Fig. 5. Qualitative results of different pose transfer algorithms.

dataset with label 0 for males and label 1 for females. The pre-trained network achieves a test accuracy of 0.995. We use this pre-trained model to compute the gender recognition rate for the generated images.

In Table 1, we evaluate our proposed algorithm on the DeepFashion dataset. The keypoints-guided baseline [55] performs well for *within distribution* target poses from DeepFashion. However, the proposed text-guided approach performs satisfactorily, as reflected in SSIM, IS, DS, and LPIPS scores. As PCKh uses keypoint coordinates, our method achieves a low PCKh score compared to the keypoint-based method, which uses precise keypoints for the target image generation. For evaluating *out of distribution* target poses, we select 50 pairs of source and target images from DeepFashion; however, we estimate the target keypoints from real-world images (outside DeepFashion) having similar poses as the original target images. As shown in Table 2, in such a case, the proposed technique achieves significantly higher SSIM and PCKh values, indicating much better structural generation for real-world pose references.

User Study: It is known that quantitative metrics do not always reflect the perceptual quality of images well [42,55] and a quantifiable metric for evaluating image quality is still an open problem in computer vision. Therefore, we also perform an opinion-based user assessment to judge the realness of the generated images. Following the similar protocol as [28,42,55], the observer needs to provide an instant decision whether an image is real or fake. We create a subset of 260 real and 260 generated images with 10 images of each type used as a practice set. During the test, 20 random images (10 real + 10 fake) are drawn from the

Table 1. Performance of pose transfer algorithms on DeepFashion.

Pose Generation Algorithm	SSIM	IS	DS	PCKh	GCR	LPIPS (VGG)	LPIPS (SqzNet)
Partially Text Guided (Ours)	0.549	3.269	0.950	0.53	0.963	0.402	0.290
Fully Text Guided (Ours)	0.549	3.296	0.950	0.53	0.963	0.402	0.289
Zhou et al. [52]	0.373	2.320	0.864	0.62	0.979	0.310	0.215
PATN [55]	0.773	3.209	0.976	0.96	0.983	0.299	0.170
Real Data	1.000	3.790	0.948	1.00	0.995	0.000	0.000

Table 2. Performance of pose transfer algorithms for real-world targets.

Pose Generation Algorithm	SSIM	IS	DS	PCKh	GCR	LPIPS (VGG)	LPIPS (SqzNet)
Partially Text Guided (Ours)	0.696	2.093	0.990	0.84	1.000	0.262	0.155
Fully Text Guided (Ours)	0.695	2.171	0.991	0.85	1.000	0.263	0.157
Zhou et al. [52]	0.615	2.891	0.931	0.52	1.000	0.271	0.182
PATN [55]	0.677	2.779	0.996	0.64	1.000	0.294	0.183
Real Data	1.000	2.431	0.984	1.00	1.000	0.000	0.000

remaining images and shown to the examiner. We compute the **R2G** (the fraction of real images identified as generated) and **G2R** (the fraction of generated images identified as real) scores from the user submissions. Our method achieves a mean G2R score of 0.6968 for submissions by 156 individual volunteers.

5.2 Ablation

We perform exhaustive ablation experiments to understand the effectiveness of different architectural components of the proposed pipeline. As shown in Table 3, refinement helps to improve SSIM, IS, and GCR scores in both partially and fully text-based approaches. Though the improvement in terms of metric values may look incremental, as shown in Fig. 6, the qualitative improvement due to the refinement operation is remarkable. Facial features play an essential role in the overall human appearance. Thus, the use of refinement is highly desirable in the pipeline. We report the rest of the ablation results with a partially text-based scheme while keeping the refinement operation intact in the pipeline.

We also explore several text embedding techniques and their effects on the generation pipeline. As shown in Table 4, the encoding methods like FastText [2] and Word2Vec [30] perform closely to BERT [7]. Thus, we can conclude that our method is robust to standard text embedding algorithms.

We also observe the effect of multi-resolution attention used in G_S . In the case of single-scale attention, we only take point-wise multiplication of the channels of the final pose encoder and the final image encoder and skip all the following supervision of the pose encoders at higher resolution levels. As shown in Table 5, multi-scale attention significantly improves majority of the evaluation metrics.

Table 3. Effects of source encoding and regressive refinement.

Source Encoding	Refinement	SSIM	IS	DS	PCKh	GCR	LPIPS (VGG)	LPIPS (SqzNet)
Keypoints	✗	0.545	3.221	0.952	0.53	0.960	0.404	0.290
Keypoints	✓	0.549	3.269	0.950	0.53	0.963	0.402	0.290
Text Embedding	✗	0.545	3.261	0.952	0.53	0.960	0.404	0.290
Text Embedding	✓	0.549	3.296	0.950	0.53	0.963	0.402	0.289
Real Data		1.000	3.790	0.948	1.00	0.995	0.000	0.000

Table 4. Effects of different text encoding methods.

Text Embedding	SSIM	IS	DS	PCKh	GCR	LPIPS (VGG)	LPIPS (SqzNet)
Multi-hot	0.558	3.228	0.953	0.60	0.970	0.388	0.274
BERT [7]	0.549	3.269	0.950	0.53	0.963	0.402	0.290
FastText [2]	0.548	3.275	0.949	0.52	0.968	0.399	0.285
Word2Vec [30]	0.550	3.251	0.949	0.52	0.973	0.401	0.289
Real Data	1.000	3.790	0.948	1.00	0.995	0.000	0.000

Table 5. Effects of multi-resolution attention.

Pose Transfer Method	SSIM	IS	DS	PCKh	GCR	LPIPS (VGG)	LPIPS (SqzNet)
Single-scale Attention Guided	0.540	3.170	0.921	0.54	0.954	0.415	0.298
Multi-scale Attention Guided	0.549	3.269	0.950	0.53	0.963	0.402	0.290
Real Data	1.000	3.790	0.948	1.00	0.995	0.000	0.000

**Fig. 6.** Qualitative results by the proposed pipeline using the partially text-guided generator with and without refinement.

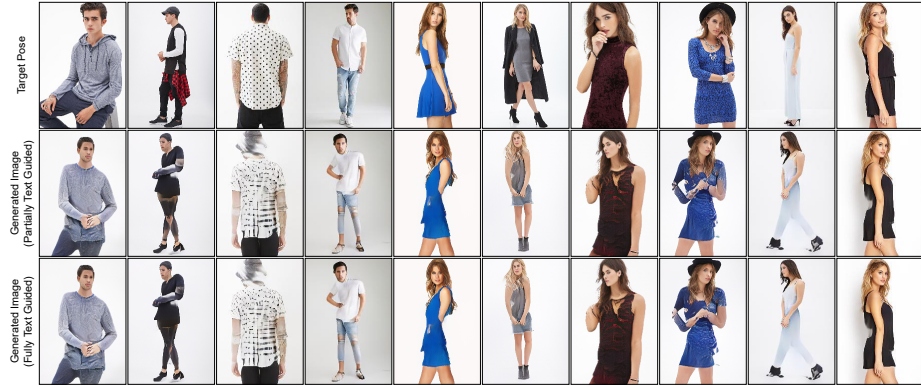


Fig. 7. Failure cases of the proposed framework.

6 Limitations

To the best of our knowledge, this is one of the earliest attempts to transfer pose using textual supervision. As shown in Sec. 5, although the results produced by the proposed approach are often at par with the existing keypoint-based baseline, it fails to perform well in some instances. When the textual description is brief and lacks a fine-grained description of the pose, the generator G_T fails to interpret the pose correctly. Some of the failed cases produced by our algorithm are shown in Fig. 7.

7 Conclusion

In this paper, we have shown that the existing keypoint-based approaches for human pose transfer suffer from a significant flaw that occasionally prevents these techniques from being useful in real-world situations when the target pose reference is unavailable. Thus, we propose a novel text-guided pose transfer pipeline to mitigate the dependency on the target pose reference. To perform the task, first, we have designed a *text to keypoints* generator for estimating the keypoints from a text description of the target pose. Next, we use a linear *refinement* network to regressively obtain a refined spatial estimation of the keypoints representing the target pose. Lastly, we *render* the target pose by conditioning a multi-resolution attention-based generator on the appearance of the source image. Due to the lack of similar public datasets, we have also introduced a new dataset DF-PASS, by extending the DeepFashion dataset with human annotations for poses.

Acknowledgment

This work was partially supported by the Technology Innovation Hub, Indian Statistical Institute Kolkata, India. The ISI-UTS Joint Research Cluster (JRC) partly funded the project.

References

1. Andriluka, M., Pishchulin, L., Gehler, P., Schiele, B.: 2D human pose estimation: New benchmark and state of the art analysis. In: The IEEE Conference on Computer Vision and Pattern Recognition (CVPR) (2014) 10
2. Athiwaratkun, B., Wilson, A.G., Anandkumar, A.: Probabilistic fasttext for multi-sense word embeddings. arXiv preprint arXiv:1806.02901 (2018) 5, 12, 13
3. Balakrishnan, G., Zhao, A., Dalca, A.V., Durand, F., Guttag, J.: Synthesizing images of humans in unseen poses. In: The IEEE Conference on Computer Vision and Pattern Recognition (CVPR) (2018) 3
4. Briq, R., Kochar, P., Gall, J.: Towards better adversarial synthesis of human images from text. arXiv preprint arXiv:2107.01869 (2021) 4
5. Cao, Z., Simon, T., Wei, S.E., Sheikh, Y.: Realtime multi-person 2D pose estimation using part affinity fields. In: The IEEE Conference on Computer Vision and Pattern Recognition (CVPR) (2017) 7
6. Chen, L., Maddox, R.K., Duan, Z., Xu, C.: Hierarchical cross-modal talking face generation with dynamic pixel-wise loss. In: The IEEE Conference on Computer Vision and Pattern Recognition (CVPR) (2019) 4
7. Devlin, J., Chang, M.W., Lee, K., Toutanova, K.: BERT: Pre-training of deep bidirectional transformers for language understanding. arXiv preprint arXiv:1810.04805 (2018) 5, 12, 13
8. Dong, C., Loy, C.C., He, K., Tang, X.: Image super-resolution using deep convolutional networks. IEEE Transactions on Pattern Analysis and Machine Intelligence (TPAMI) (2015) 3
9. Esser, P., Sutter, E., Ommer, B.: A variational U-Net for conditional appearance and shape generation. In: The IEEE Conference on Computer Vision and Pattern Recognition (CVPR) (2018) 2, 10
10. Goodfellow, I., Pouget-Abadie, J., Mirza, M., Xu, B., Warde-Farley, D., Ozair, S., Courville, A., Bengio, Y.: Generative adversarial nets. In: The Conference on Neural Information Processing Systems (NeurIPS) (2014) 3
11. Güler, R.A., Neverova, N., Kokkinos, I.: Densepose: Dense human pose estimation in the wild. In: The IEEE Conference on Computer Vision and Pattern Recognition (CVPR) (2018) 4
12. Gulrajani, I., Ahmed, F., Arjovsky, M., Dumoulin, V., Courville, A.: Improved training of Wasserstein GANs. arXiv preprint arXiv:1704.00028 (2017) 5
13. He, K., Zhang, X., Ren, S., Sun, J.: Deep residual learning for image recognition. In: The IEEE Conference on Computer Vision and Pattern Recognition (CVPR) (2016) 7
14. Iandola, F.N., Han, S., Moskewicz, M.W., Ashraf, K., Dally, W.J., Keutzer, K.: SqueezeNet: AlexNet-level accuracy with 50x fewer parameters and <0.5mb model size. arXiv preprint arXiv:1602.07360 (2016) 10
15. Ioffe, S., Szegedy, C.: Batch Normalization: Accelerating deep network training by reducing internal covariate shift. In: The International Conference on Machine Learning (ICML) (2015) 5
16. Isola, P., Zhu, J.Y., Zhou, T., Efros, A.A.: Image-to-Image translation with conditional adversarial networks. In: The IEEE Conference on Computer Vision and Pattern Recognition (CVPR) (2017) 3, 7
17. Johnson, J., Alahi, A., Fei-Fei, L.: Perceptual losses for real-time style transfer and super-resolution. In: The European Conference on Computer Vision (ECCV) (2016) 3

18. Kim, J., Kwon Lee, J., Mu Lee, K.: Accurate image super-resolution using very deep convolutional networks. In: The IEEE Conference on Computer Vision and Pattern Recognition (CVPR) (2016) [3](#)
19. Kingma, D.P., Ba, J.: Adam: A method for stochastic optimization. In: The International Conference on Learning Representations (ICLR) (2015) [9](#)
20. Lassner, C., Pons-Moll, G., Gehler, P.V.: A generative model of people in clothing. In: The IEEE International Conference on Computer Vision (ICCV) (2017) [3](#)
21. Ledig, C., Theis, L., Huszár, F., Caballero, J., Cunningham, A., Acosta, A., Aitken, A., Tejani, A., Totz, J., Wang, Z., Shi, W.: Photo-realistic single image super-resolution using a generative adversarial network. In: The IEEE Conference on Computer Vision and Pattern Recognition (CVPR) (2017) [3](#)
22. Li, K., Zhang, J., Liu, Y., Lai, Y.K., Dai, Q.: PoNA: Pose-guided non-local attention for human pose transfer. IEEE Transactions on Image Processing (TIP) (2020) [3](#)
23. Li, Y., Huang, C., Loy, C.C.: Dense intrinsic appearance flow for human pose transfer. In: The IEEE Conference on Computer Vision and Pattern Recognition (CVPR) (2019) [4](#)
24. Li, Y., Min, M., Shen, D., Carlson, D., Carin, L.: Video generation from text. In: The AAAI Conference on Artificial Intelligence (2018) [4](#)
25. Liu, W., Anguelov, D., Erhan, D., Szegedy, C., Reed, S., Fu, C.Y., Berg, A.C.: SSD: Single shot multibox detector. In: The European Conference on Computer Vision (ECCV) (2016) [10](#)
26. Liu, Z., Luo, P., Qiu, S., Wang, X., Tang, X.: DeepFashion: powering robust clothes recognition and retrieval with rich annotations. In: The IEEE Conference on Computer Vision and Pattern Recognition (CVPR) (2016) [8](#)
27. Loper, M., Mahmood, N., Romero, J., Pons-Moll, G., Black, M.J.: SMPL: A skinned multi-person linear model. ACM Transactions on Graphics (TOG) (2015) [4](#)
28. Ma, L., Jia, X., Sun, Q., Schiele, B., Tuytelaars, T., Van Gool, L.: Pose guided person image generation. In: The Conference on Neural Information Processing Systems (NeurIPS) (2017) [2](#), [3](#), [10](#), [11](#)
29. Ma, L., Sun, Q., Georgoulis, S., Van Gool, L., Schiele, B., Fritz, M.: Disentangled person image generation. In: The IEEE Conference on Computer Vision and Pattern Recognition (CVPR) (2018) [2](#), [3](#)
30. Mikolov, T., Chen, K., Corrado, G., Dean, J.: Efficient estimation of word representations in vector space. arXiv preprint arXiv:1301.3781 (2013) [5](#), [12](#), [13](#)
31. Mirza, M., Osindero, S.: Conditional generative adversarial nets. arXiv preprint arXiv:1411.1784 (2014) [3](#)
32. Nair, V., Hinton, G.E.: Rectified linear units improve Restricted Boltzmann Machines. In: The International Conference on Machine Learning (ICML) (2010) [5](#)
33. Neverova, N., Guler, R.A., Kokkinos, I.: Dense pose transfer. In: The European Conference on Computer Vision (ECCV) (2018) [4](#)
34. Pumarola, A., Agudo, A., Sanfeliu, A., Moreno-Noguer, F.: Unsupervised person image synthesis in arbitrary poses. In: The IEEE Conference on Computer Vision and Pattern Recognition (CVPR) (2018) [3](#)
35. Qiao, T., Zhang, J., Xu, D., Tao, D.: MirrorGAN: Learning text-to-image generation by redescription. In: The IEEE Conference on Computer Vision and Pattern Recognition (CVPR) (2019) [4](#)
36. Radford, A., Metz, L., Chintala, S.: Unsupervised representation learning with deep convolutional generative adversarial networks. In: The International Conference on Learning Representations (ICLR) (2016) [3](#)

37. Reed, S., Akata, Z., Yan, X., Logeswaran, L., Schiele, B., Lee, H.: Generative adversarial text to image synthesis. In: The International Conference on Machine Learning (ICML) (2016) [4](#)
38. Roy, P., Bhattacharya, S., Ghosh, S., Pal, U.: Multi-scale attention guided pose transfer. arXiv preprint arXiv:2202.06777 (2022) [7](#)
39. Roy, P., Ghosh, S., Bhattacharya, S., Pal, U., Blumenstein, M.: Scene aware person image generation through global contextual conditioning. In: The International Conference on Pattern Recognition (ICPR) (2022) [7](#)
40. Salimans, T., Goodfellow, I.J., Zaremba, W., Cheung, V., Radford, A., Chen, X.: Improved techniques for training GANs. In: The Conference on Neural Information Processing Systems (NeurIPS) (2016) [10](#)
41. Sangkloy, P., Lu, J., Fang, C., Yu, F., Hays, J.: Scribbler: Controlling deep image synthesis with sketch and color. In: The IEEE Conference on Computer Vision and Pattern Recognition (CVPR) (2017) [3](#)
42. Siarohin, A., Sangineto, E., Lathuilière, S., Sebe, N.: Deformable GANs for pose-based human image generation. In: The IEEE Conference on Computer Vision and Pattern Recognition (CVPR) (2018) [2](#), [4](#), [10](#), [11](#)
43. Simonyan, K., Zisserman, A.: Very deep convolutional networks for large-scale image recognition. In: The International Conference on Learning Representations (ICLR) (2015) [8](#), [10](#)
44. Wang, B., Zheng, H., Liang, X., Chen, Y., Lin, L., Yang, M.: Toward characteristic-preserving image-based virtual try-on network. In: The European Conference on Computer Vision (ECCV) (2018) [3](#)
45. Wang, Z., Bovik, A.C., Sheikh, H.R., Simoncelli, E.P.: Image quality assessment: From error visibility to structural similarity. IEEE Transactions on Image Processing (TIP) (2004) [10](#)
46. Yeh, R.A., Chen, C., Yian Lim, T., Schwing, A.G., Hasegawa-Johnson, M., Do, M.N.: Semantic image inpainting with deep generative models. In: The IEEE Conference on Computer Vision and Pattern Recognition (CVPR) (2017) [3](#)
47. Zanfir, M., Popa, A.I., Zanfir, A., Sminchisescu, C.: Human appearance transfer. In: The IEEE Conference on Computer Vision and Pattern Recognition (CVPR) (2018) [4](#)
48. Zhang, R., Isola, P., Efros, A.A., Shechtman, E., Wang, O.: The unreasonable effectiveness of deep features as a perceptual metric. In: The IEEE Conference on Computer Vision and Pattern Recognition (CVPR) (2018) [10](#)
49. Zhang, Y., Briq, R., Tanke, J., Gall, J.: Adversarial synthesis of human pose from text. In: The DAGM German Conference on Pattern Recognition (GCPR) (2020) [4](#), [5](#)
50. Zhao, B., Wu, X., Cheng, Z.Q., Liu, H., Jie, Z., Feng, J.: Multi-view image generation from a single-view. In: The ACM International Conference on Multimedia (MM) (2018) [3](#)
51. Zheng, H., Chen, L., Xu, C., Luo, J.: Pose flow learning from person images for pose guided synthesis. IEEE Transactions on Image Processing (TIP) (2020) [4](#)
52. Zhou, X., Huang, S., Li, B., Li, Y., Li, J., Zhang, Z.: Text guided person image synthesis. In: The IEEE Conference on Computer Vision and Pattern Recognition (CVPR) (2019) [4](#), [12](#)
53. Zhou, Y., Han, X., Shechtman, E., Echevarria, J., Kalogerakis, E., Li, D.: MakeItTalk: Speaker-aware talking-head animation. ACM Transactions on Graphics (TOG) (2020) [4](#)

54. Zhu, J.Y., Park, T., Isola, P., Efros, A.A.: Unpaired image-to-image translation using cycle-consistent adversarial networks. In: The IEEE International Conference on Computer Vision (ICCV) (2017) [3](#)
55. Zhu, Z., Huang, T., Shi, B., Yu, M., Wang, B., Bai, X.: Progressive pose attention transfer for person image generation. In: The IEEE Conference on Computer Vision and Pattern Recognition (CVPR) (2019) [2](#), [3](#), [9](#), [10](#), [11](#), [12](#)

Supplementary Material

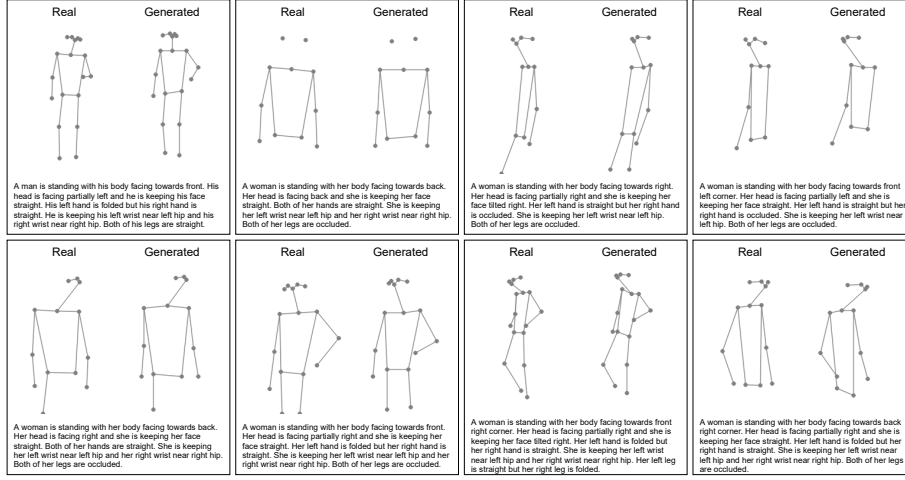


Fig. S1. Additional qualitative results of text to pose generation in stage 1. For each example, **Left:** Actual target pose (Ground Truth), **Right:** Generated pose conditioned purely on the textual description of the target pose, **Bottom:** Textual description of the target pose.



Fig. S2. Additional qualitative comparison among different pose transfer algorithms. Keypoint-guided methods tend to produce structurally inaccurate results when the physical appearance of the target pose reference significantly differs from the condition image. This observation is more frequent for the *out of distribution* target poses. The proposed text-guided technique successfully addresses this issue while retaining the ability to generate visually decent results close to the keypoint-guided baseline.

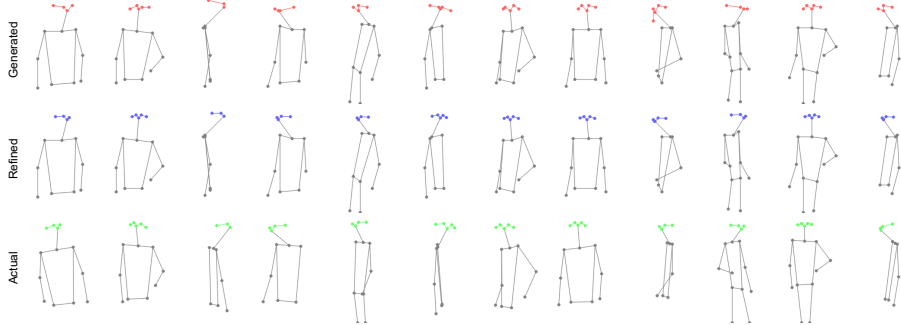


Fig. S3. Additional qualitative results of regressive refinement in stage 2. The refinement is performed specifically on the facial keypoints (marked with color). **Top:** Estimated keypoints from textual description in stage 1. **Middle:** Refined keypoints in stage 2. **Bottom:** Actual keypoints (Ground Truth).



Fig. S4. Additional qualitative results with and without refinement. **Top:** Images generated without refinement. **Middle:** Images generated with refinement. **Bottom:** Actual target images (Ground Truth). The regressive refinement (stage 2) significantly improves the final generation quality by correcting the spatial coordinates of the keypoints estimated from textual description (stage 1).

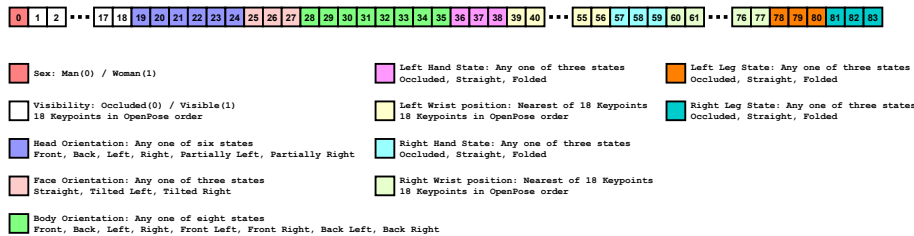


Fig. S5. The layout of the many-hot encoding vector in the proposed DF-PASS dataset.

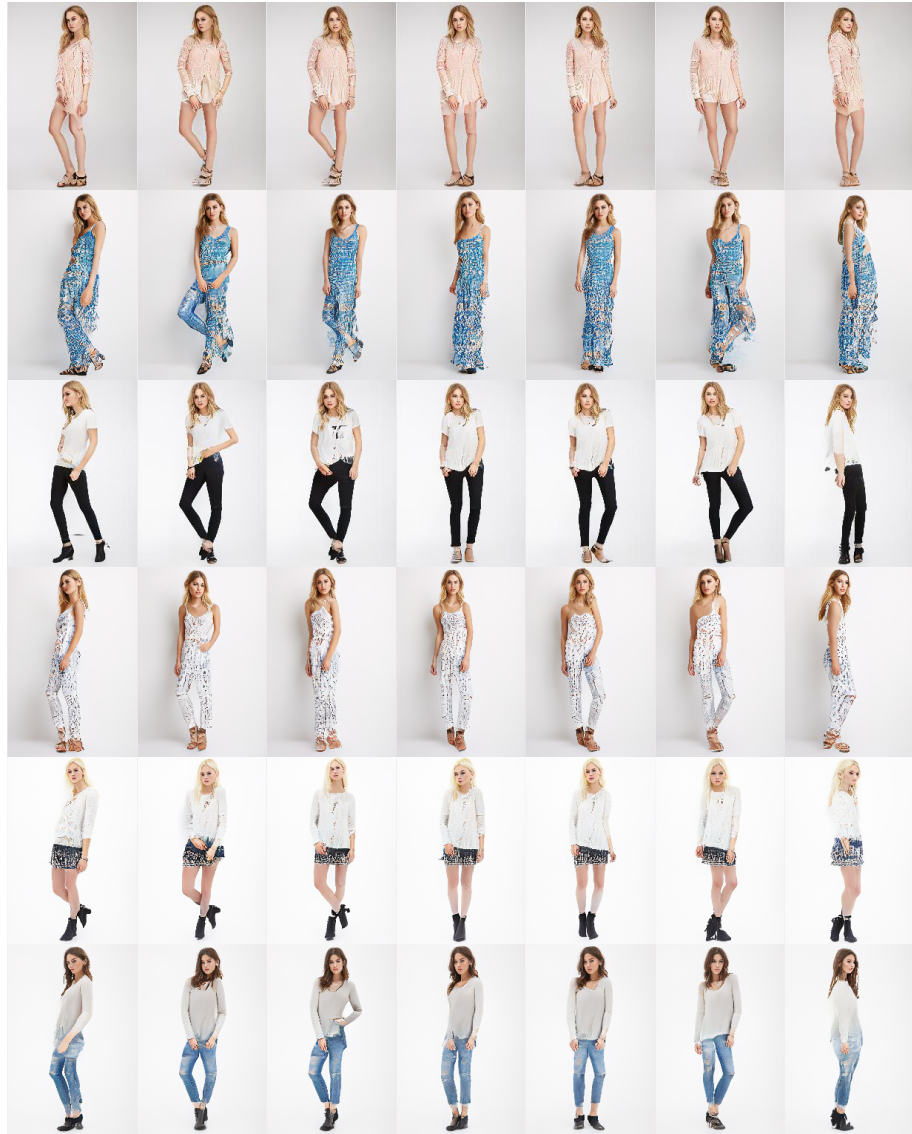


Fig. S6. Text-assisted 180° interpolation in standing pose using the proposed method.